HAL
archives-ouvertes.fr

Motion Corrected 3D Liver undersampled MRI

Felipe Yanez, Pablo Irarrazaval

▶ **To cite this version:**

Felipe Yanez, Pablo Irarrazaval. Motion Corrected 3D Liver undersampled MRI. 2014. hal-01080892v2

HAL Id: hal-01080892
https://hal.inria.fr/hal-01080892v2

Preprint submitted on 1 Jun 2015

HAL is a multi-disciplinary open access archive for the deposit and dissemination of scientific research documents, whether they are published or not. The documents may come from teaching and research institutions in France or abroad, or from public or private research centers.

L'archive ouverte pluridisciplinaire **HAL**, est destinée au dépôt et à la diffusion de documents scientifiques de niveau recherche, publiés ou non, émanant des établissements d'enseignement et de recherche français ou étrangers, des laboratoires publics ou privés.

Motion Corrected 3D Liver undersampled MRI

Felipe Yanez, and Pablo Irarrazaval

Department of Electrical Engineering and Biomedical Imaging Center,
Pontificia Universidad Católica de Chile, Santiago, Chile.

May 29, 2015

Abstract

The emergence of sparse reconstruction methods for undersampled data in Magnetic Resonance Imaging (MRI), such as Compressed Sensing (CS), have been valuable tools to accelerate data acquisition while preserving accurate image reconstruction. However, sparse reconstruction methods, including CS, are not easy to apply when there is intra-frame motion. Such is the case of free-breathing dynamic MRI in the liver. It is difficult to avoid non-rigid motion artifacts, even more so in volumetric acquisitions. To avoid these kind of artifacts, we propose a new reconstruction technique tailored for dynamic liver imaging by estimating the motion between frames to correct inconsistencies in k-space measurements. In this work, we describe how the proposed method addresses an increase in image efficiency for free-breathing dynamic 3D liver MRI, producing gains up to 6 dB with respect of traditional CS framework. Our technique can be readily extended to 3D CINE liver MRI without requiring additional information.

Index Terms: Compressed sensing, Undersampling, Sparse reconstruction, Motion correction, Non-rigid registration, Liver.

1 Introduction

Image efficiency in Magnetic Resonance Imaging (MRI), i.e. the trade-off between acquisition time and image quality, has been widely studied in the MRI community. In the past, image effi-

ciency improvements were shown to be directly related to hardware development, e.g. acquiring multiple lines in the readout after a single excitation to speed up data collection [1]. Nowadays, we are at the point where physical and physiological restrictions are the main reasons for limiting the scanning speed [2]. In this sense, the emergence of new approaches handling the imaging problem with less data than required by the Nyquist-Shannon rate seem to provide an answer for further improvements in image efficiency.

These approaches, also known as sparse reconstruction methods, rely on the idea of compressibility, which assumes redundancy in an image [3]. One sparse reconstruction method used to speed up MRI scanning time is Compressed Sensing (CS) [3, 4]. CS enables reliable image recovery for severely undersampled random measurements, if the desired signal is compressible in a known domain and the aliasing artifacts due undersampling are incoherent in the measurement domain [3, 4]. The CS framework has been used in different MRI applications, e.g. brain [5], diffusion spectrum [6], quantitative susceptibility mapping [7], and multi-contrast reconstruction [8].

CS has been also applied in dynamic MRI, where most reconstruction methods use temporal correlations of the signal. A common approach is to exploit the sparsity of the residual signal after subtracting an initial estimate [9, 10]. In this way, the signal has a sparse representation, and it is possible to achieve more accurate results. A similar problem has been also studied in the field of video compression, where video images are compressed using the similarities between different frames to achieve high efficiency. Some ideas from video compression algorithms have been used in dynamic MRI reconstructions [10].

In MRI applications, dealing with motion is also an important issue for reconstruction methods because patient's unwanted or involuntary motion during acquisition may lead to artifacts in the reconstructed images [5, 11]. The presence of motion may also reduce the sparsity of the images [11]. In this sense, a generalized motion correction framework was developed to correct non-rigid motion in the reconstructed images [12]. This framework models motion-corrupted images through the application of a matrix equation. As demonstrated in [12, 13], it is possible to reconstruct a motion-corrected image using numerical matrix inversion algorithms.

In liver MRI, it is critical to have high spatial and temporal resolution to identify small structures or to evaluate the liver parenchyma perfusion to detect focal or diffuse perfusion defects. Additionally actual volumetric technique results in poor-resolution images due to they are obtained in patients with breath-hold limitations [14]. Small structures such as tumor nodules up to 20 mm and tumor angioinvasion are hard to identify in low-quality images [15]. Increasing spatial and temporal resolution can help to detect tumors in early stages, thereby avoiding surgery and instead treating the patient with curative therapy, which provides the best possible long-term survival at a lower cost [16, 17].

Herein, we propose a compressed sensing framework tailored for free-breathing 3D liver MRI with high spatial and temporal resolution. The proposed dynamic framework incorporates a generalized non-rigid motion registration between frames [18, 19] to correct inconsistencies in k-space and increase the number of samples to recover a motion corrected image under a CS reconstruction method [11]. At each frame, the number of measurements is severely below the Nyquist-Shannon rate. Parallel imaging was used in this work, applying the proposed method independently to each coil. We performed this approach in 3D in-vivo experiments using various undersampling factors, obtaining improved signal-to-error ratios with respect to traditional CS technique [2] and accurate structural similarity with the ground truth.

2 Theory

In this section we first present the imaging problem to solve, followed by the proposed reconstruction technique.

2.1 Imaging

In dynamic MRI, the acquisition is usually done at the same respiratory position to avoid motion artifacts (Figure 1 (a)). Instead, we will consider sampling at different breathing positions, i.e. the acquired data in a respiratory cycle of T possible motion states (frames) delivers a collection of T images, as illustrated in Figure 1 (b). We assume that at a particular discrete

time $t \in \{1, \ldots, T\}$, all acquired k-space values are consistent, i.e. each frame is free of motion artifacts.

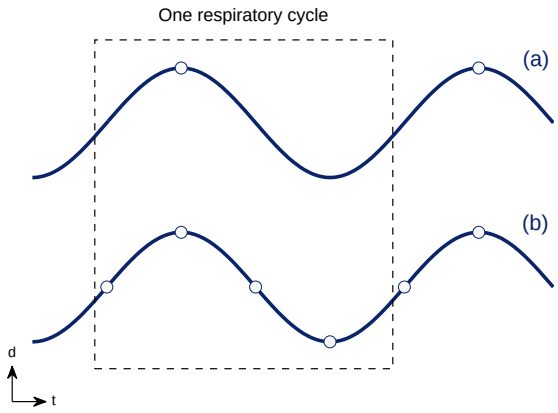

Figure 1: Representation of two acquisition approaches employed in dynamic MRI, considering measurements at different translational displacement positions across time. (a) Traditional acquisition technique, the acquired data in a respiratory cycle of T possible frames delivers a collection of few images. (b) Proposed acquisition technique, the acquired data in a respiratory cycle of T possible frames delivers a collection of T severely undersampled images.

Let us define $\mathbf{m}_t \in \mathbb{C}^N$ as the underlying vector form of the three-dimensional complex-valued true MR images in the canonical domain at discrete times $t \in \{1, \ldots, T\}$, $\mathbf{b}_t \in \mathbb{C}^P$ as the vector form of the k-space undersampled noisy measurements of $\mathbf{m}_t$ (considering $P \ll N$), and $\mathbf{e}_t \in \mathbb{C}^P$ as the corresponding acquisition noise. To facilitate notation, we will drop the subindex t, and will assume that it represents the vector form at all discrete times $t \in \{1, \ldots, T\}$. With this, the imaging procedure can be written as

$$\mathbf{b} = \mathbf{SFm} + \mathbf{e}, \tag{1}$$

where $\mathbf{F}$ is the 3D Fourier transform operator that transforms independently each frame to k-space, and $\mathbf{S}$ is the sampling operator that randomly undersamples the k-space data from each frame.

We can also describe $\mathbf{m}$ from a reference frame $\mathbf{m}_{t_0} \in \mathbb{C}^N$ by using the motion information between each frame and the reference [13]. We denote $\mathbf{V}$ as a motion operator that warps the pixels from an arbitrary reference image $\mathbf{m}_{t_0}$ to the positions at all possible times. In operator

form, this is

$$\mathbf{m} = \mathbf{V}\mathbf{m}_{t_0}, \tag{2}$$

such that Equation (1) becomes

$$\mathbf{b} = \mathbf{SFV}\mathbf{m}_{t_0} + \mathbf{e}. \tag{3}$$

As k-space has been severely undersampled ($P \ll N$), the system in Equation (3) is ill-posed, i.e. it does not satisfy the Nyquist-Shannon sampling rate. To measure the degree of undersampling, we define the acceleration factor as $R = N/P$.

2.2 Reconstruction

We propose to address the reconstruction of a motion corrected image by solving an optimization problem for a reference image $\mathbf{m}_{t_0} \in \mathbb{C}^N$, chosen from any of the T possible frames in the respiratory cycle. A comprehensive theory to tackle this problem is CS [3, 4]. We propose a second-order cone program that minimizes the regularized version of Equation (3), i.e. the ℓ^1-norm of a sparse representation of $\mathbf{m}_{t_0}$, with the data consistency constraints

$$\begin{aligned} \underset{\mathbf{m}_{t_0}}{\text{minimize}} \quad & \|\Phi\mathbf{m}_{t_0}\|_1 \\ \text{subject to} \quad & \tfrac{1}{2}\|\mathbf{SFV}\mathbf{m}_{t_0} - \mathbf{b}\|^2 < \sigma, \end{aligned} \tag{4}$$

where Φ is a sparsifying operator, e.g. wavelet, or total variation, and σ is a small positive number that controls data fidelity, usually determined by the noise level. The previous problem may be solved using an efficient conjugate gradient method [2, 20, 21].

Prior to solving the minimization problem (4), we need to find an approximation to the motion operator $\mathbf{V}$. This can be done as follows:

- Compute an initial reconstruction using a CS framework for each frame.
- Define a reference frame and estimate the motion vectors by registering all frames to the reference [22].

- Finally, define $\mathbf{V}$ using this registration to align frames to the reference, and the inverse registration function is used to warp the reference to all possible frames.

2.2.1 Initial reconstruction

For a preliminary estimation, we exploit temporal correlations assuming sparsity of the residual signal after subtraction of an initial estimate of the mean [9]. We denote the mean of the measurements as $\bar{\mathbf{b}}$. The zero-mean measurements are computed as

$$\mathbf{b}'_t = \mathbf{b}_t - \bar{\mathbf{b}}, \tag{5}$$

$\forall t \in \{1, \ldots, T\}$. A zero-mean CS recovery is applied independently to the residual of each frame $\mathbf{b}'_t$. Because of the sparsity of the residual image, we select the canonical domain as the sparse domain. The initial reconstruction is

$$\hat{\mathbf{m}}' = \arg\min_{\mathbf{m}'} \tfrac{1}{2} \left\|\mathbf{SFm}' - \mathbf{b}'\right\|^2 + \beta\|\mathbf{m}'\|_1, \tag{6}$$

where β is the regularization parameter. The initial reconstruction is computed by adding the mean image in the canonical domain to each residual estimation,

$$\hat{\mathbf{m}}_t = \hat{\mathbf{m}}'_t + \mathbf{F}^H \bar{\mathbf{b}}, \tag{7}$$

$\forall t \in \{1, \ldots, T\}$, where $\mathbf{F}^H$ is the Hermitian transpose of $\mathbf{F}$.

2.2.2 Motion vectors estimation

The reconstructed frames allow us to select a reference image. The reference frame is usually chosen at end expiration when the liver is moving less. Each preliminary estimation is registered to the reference frame using a fast and efficient adaptive regularization approach for non-rigid image registration [18]. Our registration method relies on a Bayesian formulation, where we estimate the prior distribution on parameters assuming that it is close to some given model

distribution. We constrain the prior distribution to be a Gauss-Markov random field, which allows us to solve for the prior distribution analytically and provides a fast optimization algorithm [18],

$$\mathbf{V}_t = \arg\min_{\mathbf{v}_t} \tfrac{1}{w} D(\hat{\mathbf{m}}_t, \hat{\mathbf{m}}_{t_0} | \mathbf{v}_t) + \left\| \mathbf{k}^\top \mathbf{Q} \mathbf{v}_t \right\|_1 , \tag{8}$$

$\forall t \in \{1, \ldots, T\}$, where $D(\hat{\mathbf{m}}_t, \hat{\mathbf{m}}_{t_0} | \mathbf{v}_t)$ is a similarity measure, e.g. Mutual Information, Sum of Squared Differences, or Sum of Absolute Differences, w is the weight between data consistency and penalization, $\mathbf{k}$ are the squared-root-eigenvalues of the model distribution, $\mathbf{Q}$ is a matrix containing the eigenvectors of the inverse covariance shift-invariant matrix. In a prior distribution constrained to be a Gauss-Markov random field, the eigenvalues and eigenvectors have a known form [18]. Motion operator $\mathbf{V}$ is defined by the motion vectors $\mathbf{V}_t$ obtained from the proposed registration algorithm. The motion vectors are obtained pixel-wise for every frame.

2.2.3 MC-CS recovery

To recover the motion corrected image, $\hat{\mathbf{m}}_{t_0}$, the acquired data from all the motion states (frames) $\mathbf{b}$ and the estimated motion vectors operator $\mathbf{V}$ are needed as shown in Equation (4). Considering the noise level in the λ regularization parameter, the unconstrained version of the minimization problem in Equation (4) is as follows:

$$\hat{\mathbf{m}}_{t_0} = \arg\min_{\mathbf{m}_{t_0}} \tfrac{1}{2} \left\| \mathbf{SFV}\mathbf{m}_{t_0} - \mathbf{b} \right\|^2 + \lambda \left\| \Phi \mathbf{m}_{t_0} \right\|_1 . \tag{9}$$

3 Methods

The goal of the proposed technique is to reconstruct a motion corrected 3D liver image from undersampled pseudorandom measurements. The main contribution is employing motion-corrected inconsistent k-space samples from different frames into a CS reconstruction framework to estimate a single higher quality image. To correct motion, we estimate the motion vectors between different frames. To compute the motion vectors we perform a preliminary CS reconstruction to each frame, and subsequently, we register those reconstructed images to a reference frame.

The obtained motion vectors generate the motion operator $\mathbf{V}$, which is an invertible matrix [12]. Figure 2 illustrates a block diagram with the proposed algorithm steps.

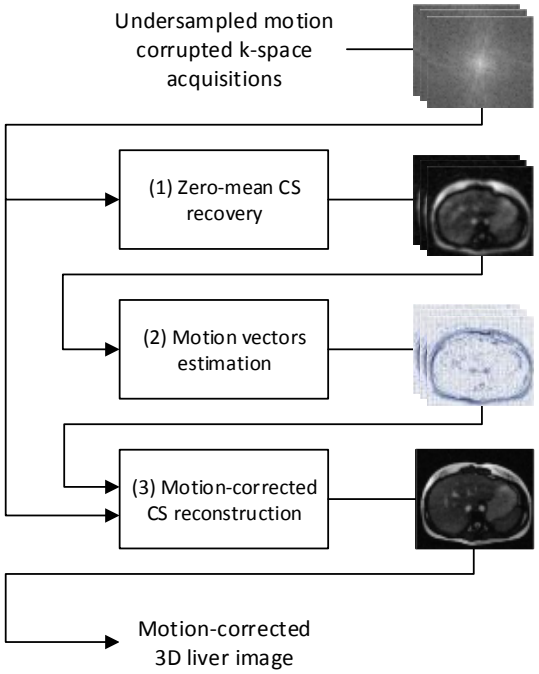

Figure 2: Block diagram of the proposed free-breathing dynamic 3D liver MRI reconstruction framework. (1) From the acquired undersampled motion corrupted samples, the mean of the data is subtracted. A CS recovery is performed to the residual, independently for each of the T frames. The estimation of each image is computed as the sum of the corresponding CS recovery with the mean image in the canonical domain. (2) The reconstructed images allows us to select a reference frame, usually chosen at end expiration where the liver is moving less. The T reconstructed frames are registered to the reference image, to compute the corresponding motion vectors. (3) The undersampled motion corrupted k-space acquisitions and the previously computed motion vectors are used to perform a motion corrected CS reconstruction to obtain a high resolution 3D liver image.

We performed a conventional 3D T1-weighted fast field echo sequence in the liver of healthy volunteers to generate the in-vivo dataset. We asked the volunteers to hold their breaths at different inspiration levels. Previously, a low-resolution image was acquired as a prescan. Informed consent was obtained from volunteers prior to imaging. A four-element body coil was used for all acquisitions using a Philips Achieva 1.5 T scanner (Philips Healthcare, Best, The Netherlands).

3.1 Reconstruction protocol

To solve Equations (9) and (6), two different ℓ^1-norm penalized non-linear conjugate gradients with fast & cheap backtracking line-search reconstruction were implemented in Matlab (R2011a, The MathWorks, Inc., Natick, MA). We used a standard personal computer to run the algorithms. In both reconstructions, we performed a maximum of 1000 conjugate gradient iterations. Equation (9), for computational efficiency, was solved using the Hermitian-symmetric form for data consistency:

$$\mathbf{V}^H\mathbf{F}^H\mathbf{S}^H\mathbf{SFV}\mathbf{m}_{t_0} = \mathbf{V}^H\mathbf{F}^H\mathbf{S}^H\mathbf{b}. \tag{10}$$

For Equations (9) and (6), we selected optimal λ and β via the computation of the L-curve criterion [23, 24]. In this case, optimal regularization parameters lie on the corner of the L-curve [23], but sometimes it is difficult to distinguish it. In these cases we used the criteria proposed by Hansen and O'Leary of choosing the point with maximum curvature to be the optimal point [24].

In Equation (9), the sparse representation is obtained via wavelet transformation. We used an especially effective and computationally efficient biorthogonal wavelet algorithm which was reported to yield high quality sparse approximations for simulated diffusion propagators [25]. In Equation (6), the sparse representation is in the canonical domain.

3.2 In-vivo experiments

We simulated a free-breathing acquisition in order to have a ground truth. By performing a conventional breath-held 3D T1-weighted fast field echo sequence with fully sampled cartesian trajectory in the liver of four healthy volunteers, we generated the in-vivo dataset. We asked the volunteers to hold their breaths at five different inspiration levels.

For liver imaging, a four-element body coil was used. The measurements were obtained with the following parameters: TR = 4.1 ms, TE = 1.95 ms, FOV = $160 \times 224 \times 150$ mm^3, FA = 10^o, slice thickness = 10 mm, dynamic scans = 8, spatial resolution = 2 mm isotropic, dynamic scan time = 14.8 s.

The coil sensitivity maps were estimated by preliminarily acquiring a fully-sampled low-resolution image prior to the 3D T1-weighted fast field echo sequence. Both acquisitions had identical previously defined scan parameters. A smoothing filter was applied to the low-resolution images from each coil. The estimated maps were found to be the normalization of each smoothed low-resolution image by computing the sum-of-squares of all coil images.

Undersampled k-space data were obtained with different sampling pattern for each frame, which were generated using a Monte Carlo algorithm with minimum peak interference according to a particular acceleration factor (R) [2]. The random sampling pattern is based on a polynomial variable density function, i.e. the low-frequency regions are more dense than the higher frequency regions. The number of samples from each frame is determined by the probability density function (pdf) and the sampling factor (R). We also enabled a sampling pattern that does not require a pdf. In-vivo experiments were performed at various R.

To compute $\mathbf{V}$, the CS reconstructions from each receiver coil were combined using the sum of squares prior to registration. The reference image (frame) is chosen from previous combined reconstructions. We set as the reference the most common respiratory motion state at end expiration when the liver is moving less. All CS estimations are non-rigidly registered to the reference using an adaptive image registration algorithm [18]. We used this registration to align frames to the reference, and the inverse registration function to warp the reference to all possible frames. Motion operator $\mathbf{V}$ is constructed with these two functions. We performed the registration algorithm that solves Equation (8) using the Mutual Information similarity measure.

We used the motion operator $\mathbf{V}$ and undersampled k-space data to reconstruct the underlying motion corrected 3D liver image using the proposed technique. To test accuracy in reconstructions, we considered the signal-to-error ratio (SER)

$$SER = 20 \log_{10} \left(\frac{\|\mathbf{y}\|}{\|\mathbf{x} - \mathbf{y}\|} \right), \tag{11}$$

and the complex wavelet structural similarity (CW-SSIM) index [26] defined as

$$CW\text{-}SSIM = \frac{2|\sum_{i=1}^{n} c_{x,i}c_{y,i}^{*}| + K}{\sum_{i=1}^{n}|c_{x,i}|^2 + \sum_{i=1}^{n}|c_{y,i}|^2 + K}, \tag{12}$$

where in both cases $\mathbf{x} \in \mathbb{R}^m$ and $\mathbf{y} \in \mathbb{R}^m$ are the absolute value vector representation of the estimated image and the true image, respectively. In the CW-SSIM index, $\mathbf{c}_x \in \mathbb{C}^n$ and $\mathbf{c}_y \in \mathbb{C}^n$ represent the wavelet coefficients of images $\mathbf{x}$ and $\mathbf{y}$; $()^*$ represents the complex conjugation operation; and K represents a small positive constant to achieve accurate performance in local low contrast regions [26].

4 Results

The proposed technique was tested on the in-vivo dataset with breath-held 3D liver MRI data simulating five different motion states. The performance of the proposed Motion-Corrected Compressed Sensing technique (MCCS) was compared against a traditional CS reconstruction (CS) [2].

4.1 Regularization parameters

We selected optimal settings for the MCCS and CS frameworks. Computations of the L-curve were performed on the in-vivo dataset using several reduction factors (R), and selecting the operating point with maximum curvature.

Figure 3 illustrates the L-curve and curvature of the regularization parameters for MCCS and CS with 5-fold acceleration. We used 15 different tunning parameters. For both cases, setting $\lambda = 0.01$ and $\beta = 0.002$, as in (a), yielded to an under-regularized image reconstruction, whereas using $\lambda = 0.5$ and $\beta = 0.2$, as in (c), resulted in an over-regularized image reconstruction. For both cases, the second column in Figures 3 illustrates the computation of the curvature as function of the regularization parameter, where λ_{opt} and β_{opt} were the operating point that maximized the curvature. Therefore, $\lambda_{opt} = 0.1$ and $\beta_{opt} = 0.04$, as in (b), were the optimal

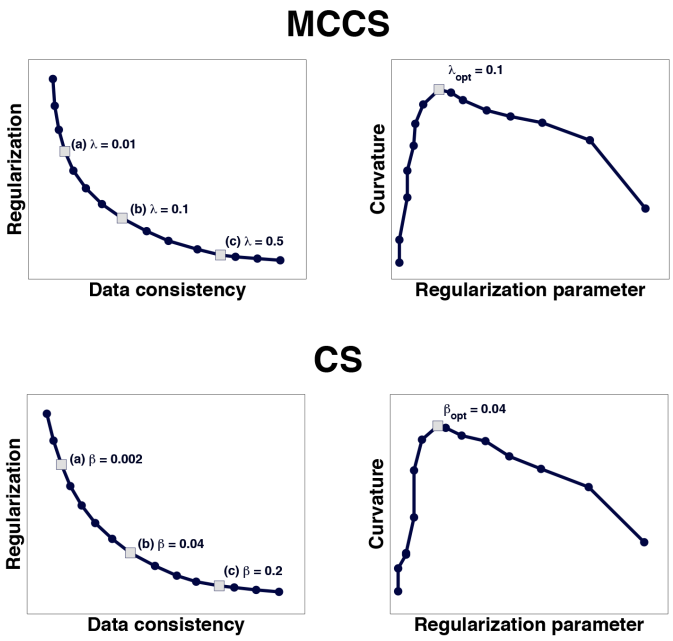

Figure 3: Optimal parameter selection for MCCS and CS. The L-curve was computed on the left, where the X-axis represents the data consistency term, and the Y-axis represents the regularization term. On the right, we illustrate the computation of the curvature as function of the regularization parameter.

regularization parameters. All MCCS and CS reconstructions are performed with these optimal settings.

4.2 Image recovery

The proposed technique was tested on the in-vivo dataset with breath-held 3D liver MRI data simulating a free-breathing acquisition. This could represent a realistic case if we consider that with a 5x undersampling, where the total scan time per frame would be 3 s during which we assume that the liver does not move significantly. This means a scan time per frame in the range of 1 to 4 s, depending on the undresampling rate.

The ground truth, fully-sampled image is illustrated in Figure 4 displaying a coronal slice. The first out of eight frames was set as the reference. The performance of the proposed MCCS technique, tailored for free-breathing acquisitions, was compared against a traditional CS reconstruction of the reference frame. In our experiments, we downsampled the data according to different sampling patterns ($\mathbf{S}$) using acceleration factors from $R = 4$ to $R = 20$. Figure 4

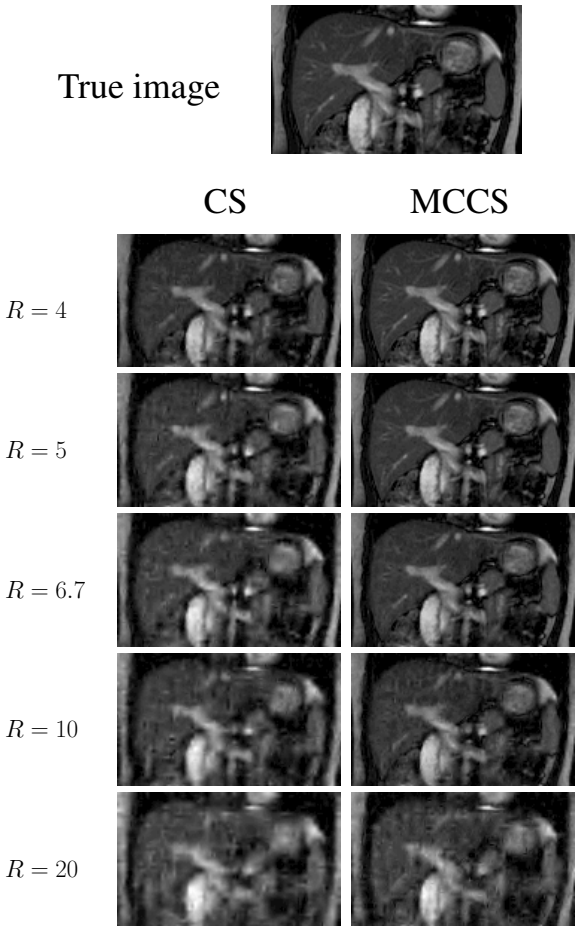

Figure 4: Results obtained using the MCCS and CS methods at different R.

presents the traditional CS and proposed MCCS reconstructions at reduction factors of 4, 5, 6.7, 10 and 20. For the CS reconstructions, motion artifacts due to severely undersampling k-space became more evident as R increases. Preservation of sharp edges and correction of motion artifacts can be observed in the MCCS reconstructions.

4.3 Computation of ratios

The proposed MCCS reconstruction method with optimal settings at different acceleration factors was compared against a traditional CS framework. Figure 5 illustrates the SER as function of R. Reconstructions obtained with the proposed technique reported more accurate results, with SER gains up to 6 dB compared to the traditional CS framework.

Four different volunteers were scanned to create the underlying dataset. To test the robustness

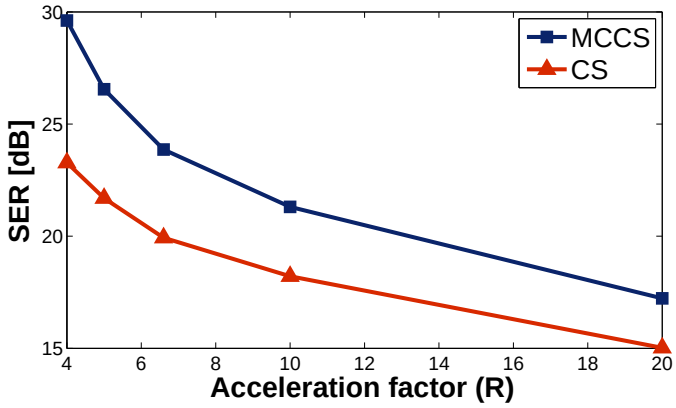

Figure 5: Computation of the reconstruction SER for the proposed motion-corrected CS recovery (MCCS) and traditional CS framework (CS) at different acceleration factors (R) using the 3D-liver in-vivo dataset.

of the proposed technique, the CW-SSIM index between the ground truth and each MCCS reconstruction was computed for several reduction factors. Figure 6 illustrates a plot of the mean and standard deviation of the index as a function of R. Reported results show that the proposed technique is stable under high reduction factors.

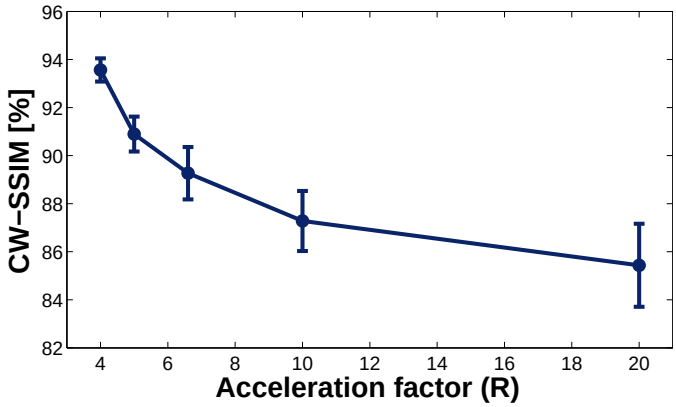

Figure 6: Computation of the reconstruction CW-SSIM index using the MCCS technique for the 4 volunteers of the dataset at different acceleration factors (R). The mean CW-SSIM index of the 4 MCCS reconstructions is illustrated as a function of R, with its respective standard deviation.

5 Discussion

We proposed a motion corrected reconstruction technique tailored for dynamic 3D liver under-sampled MRI. The main contribution is to employ motion-corrected inconsistent k-space samples

from different motion states (frames) of the liver into a CS reconstruction framework to estimate a motion corrected image [11]. As shown in the results, this technique achieved accurate and reliable reconstructions in the in-vivo experiments (Figures 4, 5 and 6). Although we are not testing our method with truly free-breathing data, we are confident that the results hold because for most of the respiratory cycle the quasi-static assumption for the liver is valid, and therefore we will have intra-frame k-space consistency most of the time.

To correct motion, we estimated the motion vectors between different motion states (frames) by using CS to reconstruct each frame and by registering these images to a reference. The CS framework recovers structured images by relying on compressibility, i.e. high contrast components are chosen over low contrast (Figure 4). In addition, registration also favors high contrast samples, which leads to decreased signal-to-error ratios outside the liver (higher contrast region) [11, 27].

We have used an adaptive non-rigid registration algorithm [18] to estimate the inter-frame motion between different frames. A source of improvement to the current theory may be to estimate motion vectors within neighboring frames in the form of a linear dynamical system instead of estimating them with respect to a single reference motion state [27].

The proposed method can be extended to 3D CINE liver MRI as an approach for applications where the respiratory signal can be used as a motion surrogate signal, such as is done in coronary MR angiography [28]. In coronary MR angiography, spatial resolution is bounded by breath-hold acquisition (15–20 s), but with the emergence of navigator techniques, the spatial resolution is improved by correcting free-breathing acquisitions [28]. Using motion corrupted data (avoiding external navigator), a 3D CINE liver MR image may be generated from the motion corrected image obtained in this work. As previously discussed, to reconstruct the motion corrected image $\hat{\mathbf{m}}_{t_0}$, we need to solve Equation (9). By employing the acquired data from all the frames $\mathbf{b}$ and the estimated motion vector operator, the 3D CINE liver is

$$\hat{\mathbf{m}} = \mathbf{V}\hat{\mathbf{m}}_{t_0}. \tag{13}$$

Equation (13) shows how to generate the whole time sequence, where an accurate estimation of the respiratory signal may be obtained through rigid registration in the head-feet (H-F) direction of a region of interest (ROI) including the liver.

6 Conclusion

We have presented a recovery algorithm tailored for free-breathing dynamic 3D liver MRI, which demonstrated an increase in imaging efficiency while reducing acquisition time and removing non-rigid motion artifacts. In the in-vivo experiments, our framework produced improved SERs with respect to traditional CS technique (with gains up to 6 dB), and accurate CW-SSIM indexes in comparison with the ground truth. These results suggest that it is feasible to achieve high speedups in acquisition time and remove motion artifacts without diminishing image quality.

Acknowledgments

The authors would like to thank Michael Santoro, Cristian Tejos, Marcelo E. Andia, and Carlos Lizama for comments on earlier versions of this manuscript. The authors acknowledge financial support from CONICYT (Anillo ACT 079), FONDECYT 1100529, and MISTI MIT-PUC 2012.

References

[1] G. Wright. Magnetic resonance imaging. *IEEE Signal Process. Mag.*, 14(1):56–66, 1997.

[2] M. Lustig, D. Donoho, and J.M. Pauly. Sparse MRI: The application of compressed sensing for rapid MR imaging. *Magn. Reson. Med.*, 58(6):1182–1195, 2007.

[3] E.J. Candes, J. Romberg, and T. Tao. Robust uncertainty principles: exact signal reconstruction from highly incomplete frequency information. *IEEE Trans. Inform. Theory*, 52(2):489–509, 2006.

[4] D. Donoho. Compressed Sensing. *IEEE Trans. Inform. Theory*, 52(4):1289–1306, 2006.

[5] M. Lustig, D. Donoho, J. Santos, and J. Pauly. Compressed Sensing MRI. *IEEE Signal Process. Mag.*, 25(2):72–82, 2008.

[6] B. Bilgic, K. Setsompop, J. Cohen-Adad, A. Yendiki, L.L. Wald, and E. Adalsteinsson. Accelerated diffusion spectrum imaging with compressed sensing using adaptive dictionaries. *Magn. Reson. Med.*, 68(6):1747–1754, 2012.

[7] F. Yanez, A.P. Fan, B. Bilgic, C. Milovic, E. Adalsteinsson, and P. Irarrazaval. Quantitative Susceptibility Map Reconstruction via Total Generalized Variation Regularization. In *3rd International Workshop on Pattern Recognition in Neuroimaging*, pages 203–206, Philadelphia, PA, USA, June 2013.

[8] B. Bilgic, V.K. Goyal, and E. Adalsteinsson. Multi-contrast reconstruction with bayesian compressed sensing. *Magn. Reson. Med.*, 66(6):1601–1615, 2011.

[9] H. Jung, K. Sung, K.S. Nayak, E.Y. Kim, and J.C. Ye. k-t FOCUSS: A general compressed sensing framework for high resolution dynamic MRI. *Magn. Reson. Med.*, 61(1):103–116, 2009.

[10] H. Jung and J.C. Ye. Motion estimated and compensated compressed sensing dynamic magnetic resonance imaging: what we can learn from video compression techniques. *Int. J. Imaging. Syst. Technol.*, 20(2):81–98, 2010.

[11] M. Usman, D. Atkinson, F. Odille, C. Kolbitsch, G. Vaillant, T. Schaeffter, P.G. Batchelor, and C. Prieto. Motion corrected compressed sensing for free-breathing dynamic cardiac MRI. *Magn. Reson. Med.*, 70(2):504–516, 2012.

[12] P.G. Batchelor, D. Atkinson, P. Irarrazaval, D. Hill, J. Hajnal, and D. Larkman. Matrix description of general motion correction applied to multi-shot images. *Magn. Reson. Med.*, 54(5):1273–1280, 2005.

[13] C. Prieto, P.G. Batchelor, D.L. Hill, J.V. Hajnal, M. Guarini, and P. Irarrazaval. Reconstruction of undersampled dynamic images by modeling the motion of object elements. *Magn. Reson. Med.*, 57(5):939–949, 2007.

[14] H. Chandarana, T. Block, J. Stepancic, D.K. Sodickson, and R. Otazo. Contrast-enhanced free-breathing perfusion weighted MR imaging of the whole-liver with high spatial and temporal resolution. In *Proc. Intl. Soc. Mag. Reson. Med. 20*, page 4009, Melbourne, Australia, May 2012.

[15] H. Chandarana, E. Robinson, C.H. Hajdu, L. Drozhinin, J.S. Babb, and B. Taouli. Microvascular invasion in hepatocellular carcinoma: is it predictable with pretransplant MRI? *AJR Am. J. Roentgenol.*, 196(5):1083–1089, 2011.

[16] J.I. Lee, J.W. Lee, Y.S. Kim, Y.A. Choi, Y.S. Jeon, and S.G. Cho. Analysis of survival in very early hepatocellular carcinoma after resection. *J. Clin. Gastroenterol.*, 45(4):366–371, 2011.

[17] W.E. Naugler and A. Sonnenberg. Survival and cost-effectiveness analysis of competing strategies in the management of small hepatocellular carcinoma. *Liver Transpl.*, 16(10):1186–1194, 2010.

[18] A. Myronenko. *Non-rigid Image Registration: Regularization, Algorithms and Applications.* PhD thesis, Department of Science & Engineering School of Medicine, Oregon Health & Science University, Portland, OR, U.S.A., June 2010.

[19] D.L.G. Hill, P.G. Batchelor, M. Holden, and D.J. Hawkes. Medical image registration. *Phys. Med. Biol.*, 46(3):R1–R45, 2001.

[20] S. Becker, J. Bobin, and E.J. Candes. NESTA: A fast and accurate first-order method for sparse recovery. *SIAM J. Imaging Sciences*, 4(1):1–39, 2011.

[21] S. Boyd and L. Vandenberghe. *Convex Optimization.* Cambridge University Press, 2004.

[22] P. Irarrazaval, R. Boubertakh, R. Razavi, and D. Hill. Reconstruction of Undersampled Dynamic Images Based on Time Frame Registration. *Magn. Reson. Med.*, 54(1):1207–1215, 2005.

[23] P.C. Hansen. Analysis of discrete ill-posed problems by means of the L-curve. *SIAM Rev.*, 34(4):561–580, 1992.

[24] P.C. Hansen and D.P. O'Leary. The use of the L-curve in the regularization of discrete ill-posed problems. *SIAM J. Sci. Comput.*, 14(6):1487–1503, 1993.

[25] S.L. Merlet, M. Paquette, R. Deriche, and M. Descoteaux. Ensemble average propagator reconstruction via compressed sensing: Discrete or continuous bases? In *Proc. Intl. Soc. Mag. Reson. Med. 20*, page 2277, Melbourne, Australia, May 2012.

[26] M.P. Sampat, Z. Wang, S. Gupta, A.C. Bovik, and M.K. Markey. Complex wavelet structural similarity: a new image similarity index. *IEEE Trans. Image Process.*, 18(11):2385–2401, 2009.

[27] S.M. Asif, L. Hamilton, M. Brummer, and J. Romberg. Motion-adaptive spatio-temporal regularization for accelerated dynamic MRI. *Magn. Reson. Med.*, 70(3):800–812, 2012.

[28] M. Stuber, R.M. Botnar, P.G. Danias, K.V. Kissinger, and W.J. Manning. Submillimeter three-dimensional coronary MR angiography with real-time navigator correction: comparison of navigator locations. *Radiology*, 212(2):579–587, 1999.